Mon. Not. R. Astron. Soc. **261,** 175–184 (1993)

Multicolour surface photometry of NGC 4486 (M87) and its jet★

W. W. Zeilinger,[1] P. Møller[1] and M. Stiavelli[1,2]

[1]*European Southern Observatory, Karl Schwarzschild Straße 2, D-8046 Garching bei München, Germany*
[2]*Scuola Normale Superiore, Piazza dei Cavalieri 7, I-56100 Pisa, Italy*

Accepted 1992 September 2. Received 1992 July 6; in original form 1991 December 17

ABSTRACT

High-resolution *UBVRI* surface photometry of the nearby elliptical NGC 4486 (M87) is presented. The subtraction of the contributions of the unresolved nuclear component and the jet structure allows an accurate study also of the inner galaxy regions. The major axis of the core isophotes is found to be aligned with the jet axis, while in the region > 3 arcsec the isophotes are, on the contrary, nearly perpendicular to it. On the basis of photometry performed on the isolated jet structure, a change of the spectral index at the position of knot A onwards is found to be significant at the 3σ level. In addition, the radio–optical spectral index in the eastern radio lobe is shown to steepen in the surroundings of the hotspot. The available kinematic data are found to have insufficient resolution to be constrained by the photometric results to verify the presence of a supermassive black hole.

Key words: galaxies: individual: NGC 4486 – galaxies: jets – galaxies: photometry.

1 INTRODUCTION

The nearby E0 galaxy NGC 4486 (M87) has been the subject of many investigations regarding not only the conspicuous jet structure or the 'point-source' nuclear component but also its global morphology. In fact, excluding the core region, its luminosity profile closely follows an $r^{1/4}$ law and the isophotes show no significant deviations from pure ellipses. Most of the previous high-resolution work, however, was done on photographic material (see Carter & Dixon 1978 for a review, and also de Vaucouleurs & Nieto 1978, 1979). Most of the studies based on CCD surface photometry, namely *BVR* surface photometry using an SIT CCD combination (Young et al. 1978), *BVRI* (Boroson, Thompson & Shectman 1983), *UBR* (Davis et al. 1985; Peletier et al. 1990) and *BR* CCD surface photometry (Jedrzejewski 1987), are characterized by typical seeing conditions.

Because of the predominant jet structure and a central cusp in the luminosity profile, it is difficult to perform reliable surface photometry. Thus most of the published data exclude the innermost regions. In this paper, we present *UBVRI* high-resolution surface photometry of NGC 4486, having subtracted the contributions of the jet and the central cusp. We have also isolated the jet from the galaxy image and obtained photometry of single jet structures ('knots') in order to determine their spectral indexes in the optical wavelength region.

★Based on observations collected at the NOT, La Palma and ESO, La Silla (Chile).

2 OBSERVATIONS AND DATA REDUCTION

NGC 4486 was observed at the 2.5-m Nordic Telescope (NOT) in the *VRI* bands and at the ESO/MPI 2.2-m telescope using *UBVR* filters of the Bessel system and the Gunn *i* and *z* filters.

2.1 NOT 2.5-m observations

Observations were carried out on the NOT 2.5-m telescope, using the Stockholm Tektronix TK512-011 512×512 pixels CCD camera which has a pixel size of 27×27 μm^2. The scale on the detector is 0.20 arcsec pixel^{-1}. The observations were performed in the period 1991 May 18–20. A series of flat-field images were obtained of blank regions on the sky for each filter. Individual flat fields show large-scale differences of the order of < 2 per cent. The Stockholm CCD has a well-documented non-linearity curve (Kjeldsen 1990). We applied the necessary corrections as derived by Kjeldsen, which resulted in a peak-to-peak correction of ± 5 per cent, hence a total shift in the calibration of 0.1 mag over a range of 7 mag. The log of observations is given in Table 1. The seeing was measured by fitting Gaussians to the star-like images on the galaxy frames. The FWHM values obtained clustered in two groups, one probably corresponding to globular clusters and one to stars. The values given in the tables refer to the values obtained from the 'star' group.

Table 1. Observing log.

filter	telescope	exp. time [s]	seeing FWHM [″]	date
U	ESO/MPI	600	1.35*	June 8, 1991
U	ESO/MPI	1200		June 8, 1991
B	ESO/MPI	300	1.37*	June 8, 1991
B	ESO/MPI	600		June 8, 1991
V	ESO/MPI	120	1.22*	June 8, 1991
V	ESO/MPI	60		June 8, 1991
V	NOT	300	0.62	May 18, 1991
R	NOT	300	0.60	May 18, 1991
R	ESO/MPI	240	1.40*	Feb. 4, 1992
R	ESO/MPI	180		Feb. 6, 1992
I	NOT	300	0.56*	May 18, 1991
I	NOT	300		May 18, 1991
Gunn i	ESO/MPI	6×180	1.50*	Feb. 8, 1992
Gunn z	ESO/MPI	120	1.15*	June 8, 1991
Gunn z	ESO/MPI	240		June 8, 1991

Note: *average value for the combined image.

2.2 ESO/MPI 2.2-m EFOSC2 observations

Direct images of NGC 4486 were obtained with EFOSC2 at the Cassegrain focus of the ESO/MPI 2.2-m telescope using a coated Thomson 1024 × 1024 pixel CCD with a pixel size of 19 × 19 μm^2. The scale is 0.332 arcsec $pixel^{-1}$, yielding a field of 5.7 × 5.7 $arcmin^2$. Using flat-field and dark frames as a test, the CCD showed no effects of non-linearity within the signal range of interest. The observations were performed in the course of two observing runs in 1991 June and 1992 February. The log of observations is given in Table 1. The seeing was measured, as in the case of the NOT observations, on star-like images on the respective galaxy frames. Standard procedures for bias, dark-current and flat-field correction were applied. Fringes were detected only in the Gunn *i* and *z* frames. The flat fields were usually capable of correcting the images to ≈ 1 per cent accuracy. The respective single images of each filter were aligned with each other using star-like images in the field and then added. The alignment was usually better than 0.08 pixel. In the process of adding the single images, cosmic ray hits were also removed by comparing the respective pixel values of the frames to be added.

2.3 Photometric calibration

The background level was determined for each frame by measuring the intensity at the borders of the CCD frame. Because of the small field of the NOT CCD, the respective determinations were still influenced by the contribution of galaxy light and therefore needed a further adjustment. In both observing runs *UBVRI* photometric standard stars (Landolt 1985) were also observed, although for the observations the meteorological conditions were not photometric during the observing run at ESO. On the contrary, both nights of the NOT observing run were photometric. However, we conservatively estimate a global photometric accuracy of ±0.05 mag, which also includes possible residuals from the correction of the documented non-linearity effect, and flat-fielding errors for the NOT data. For the *U*- and *B*-band EFOSC2 frames, the calibration was obtained directly on the galaxy images using aperture-photometry data compiled by Longo & de Vaucouleurs (1983, 1985). Examining the filter transmission curves and CCD response curves, we found that the effective wavelength of the EFOSC2 Gunn *z* frame was not significantly different from the NOT *I* band. For this reason we combined the two data sets in order to obtain radially more extended data. The typical sky brightness levels were found to be $\mu_U = 21.81$, $\mu_B = 21.96$, $\mu_V = 21.83$, $m_R = 20.50$, $m_i = 20.15$, $m_z = 20.10$ mag $arcsec^{-2}$ for the EFOSC2 data and $\mu_V = 20.42$, $\mu_R = 20.20$, $\mu_I = 19.10$ mag $arcsec^{-2}$ for the NOT frames.

3 RESULTS

The fact that NGC 4486 possesses an unresolved nuclear component and a prominent jet structure clearly influences the light distribution in this region, and this results in artefacts in the analysis of the isophotes. Therefore we attempted to isolate these components in order to analyse only the underlying stellar component of the galaxy. Furthermore, in order to exclude possible artefacts in the measurements caused by one isophote analysis program, several dedicated surface photometry reduction packages were tested. The results were found to be in very good agreement and no significant dependence on the reduction package was detected (Stiavelli, Prugniel & Zeilinger 1991). The images of NGC 4486 were analysed using the surface photometry reduction package PLEINPOT (Prugniel 1989). In particular, the isophote parameters ellipticity $[\varepsilon = 1 - (b/a)]$, position angle of the major axis (PA) and the Fourier coefficients a_4 and b_4, together with the surface brightness of the respective isophote, were derived as a function of radius.

3.1 The light distribution of NGC 4486

In the case of the *V* and *R* wavebands, where both EFOSC2 and NOT images are available, an offset of ≈ 0.1 mag was applied in order to match the two data sets. The respective luminosity profiles then agreed in the overlapping region within ±0.02 mag. We were therefore able to obtain an extended profile by combining the EFOSC2 for the outer part and the NOT data for the inner part of the galaxy profile. This combination technique helped to overcome problems in the sky subtraction which were present especially in the NOT frames because of their limited field. By combining the respective EFOSC2 *V* and *R* frames taken with offset centres, we were able to obtain an effective field of 7–8 arcmin, corresponding to about 5 arcmin from the centre of M87 to the edge. By comparing the data of different wavebands, we additionally checked that no spurious colour gradients are present. The *V* profile is found to be in very good agreement with de Vaucouleurs & Nieto (1978) and Young et al. (1978).

In order to determine the behaviour of the light distribution of the underlying stellar component in the central region, it is necessary to subtract first the unresolved point-like nuclear source. The subtraction of this component was carried out by fitting multiple Gaussians to the core region and defining as nucleus the component with a FWHM ≤ 0.6 arcsec for the NOT images and FWHM ≤ 1.4 arcsec for the

EFOSC2 images which were derived from the respective measured seeing FWHM. The decomposition procedure turned out to be very sensitive to the seeing conditions. In general, the results of the NOT images were found to be more reliable because of their better seeing. For the NOT frames we also tested an extrapolation of the galaxy light profile by means of a power law down to $r=0$ arcsec, obtaining consistent results. In the case of the EFOSC2 B images, the image with the best seeing was used, rather than the combined frame. For the U band the seeing for the two images was comparable and we used the combined frame.

Fig. 1 displays the *UBVRI* luminosity profiles together with the colour gradients $(U-R)$, $(U-B)$, $(B-V)$, $(B-R)$, $(V-R)$ and $(V-I)$. The colour gradients were derived by degrading the luminosity profile having the better seeing to that of the worse one. The profiles were truncated in the centre at the final seeing radius. The profiles show that the outer regions are systematically bluer. The *UBVRI* profiles compared with the respective data of Young et al. (1978), Boroson et al. (1983) and Peletier et al. (1990) are presented in Fig. 2. The *UBV* profiles agree within 0.1 mag. The systematically larger residuals of Boroson et al. (1983) and Peletier et al. (1990) in the inner 5-arcsec region may be attributed to the fact that they did not subtract the nuclear component. The small-scale variations in the inner 2-arcsec region are due to seeing effects. There are larger differences in the R and I bands. There is only relatively good agreement with Peletier et al. (1990) with residuals <0.1 mag. The residuals are found to remain constant in the relevant region of the galaxy.

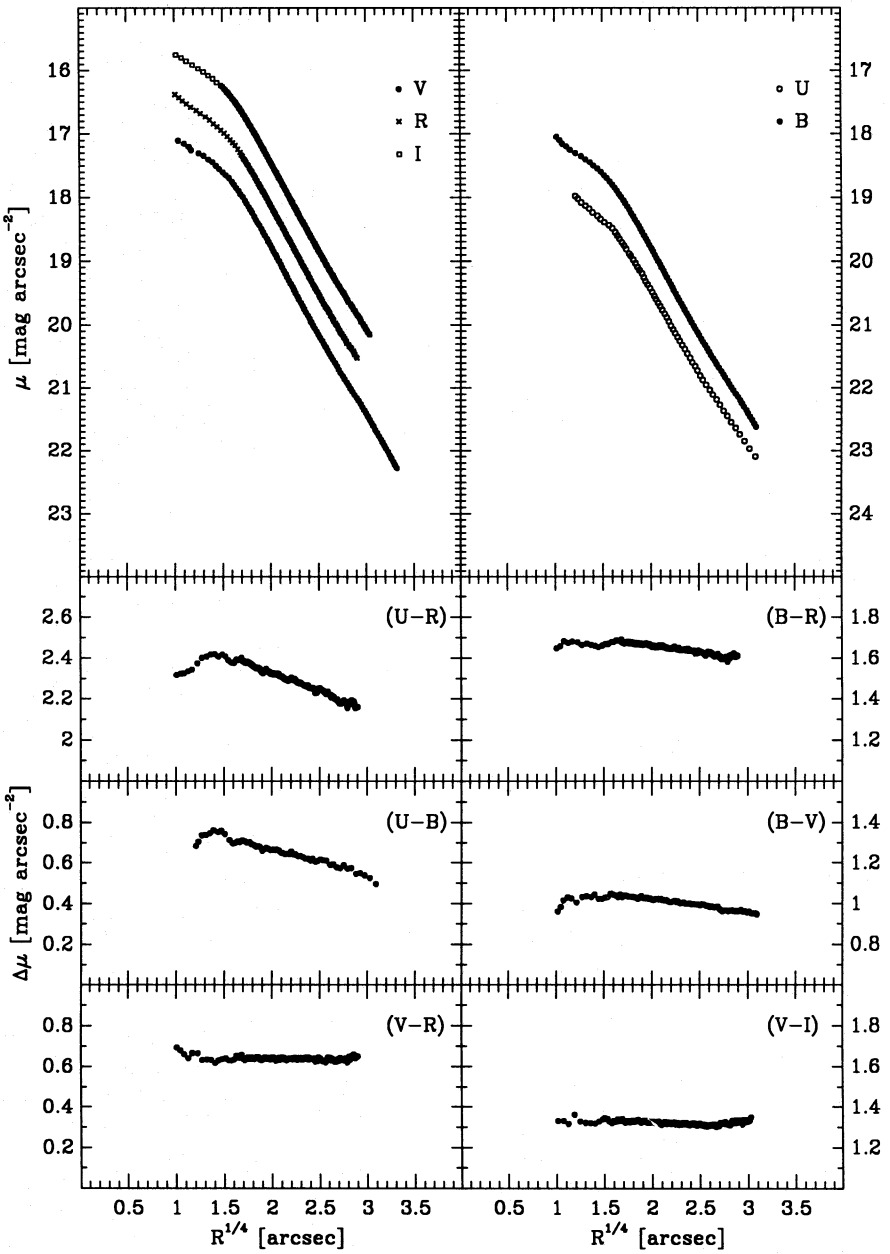

Figure 1. *UBVRI*-band surface brightness profiles together with the $(U-R)$, $(B-R)$, $(U-B)$, $(B-V)$, $(V-R)$ and $(V-I)$ colour gradients. The profiles are plotted as a function of distance from the galaxy centre rebinned to the $r^{1/4}$ scale.

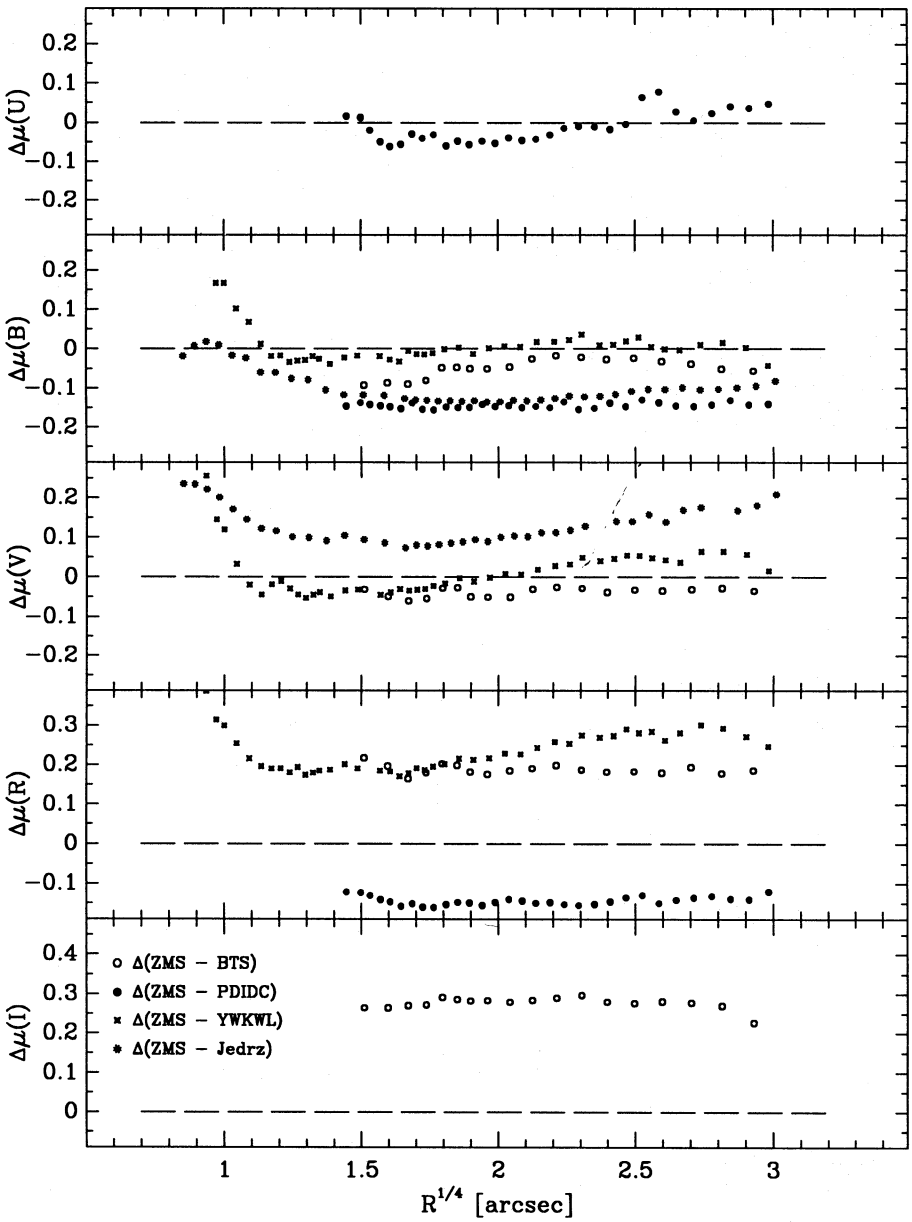

Figure 2. *UBVRI*-band profiles compared with the respective profiles of Boroson et al. (BTS), Jedrzejewski (Jedrz), Peletier et al. (PDIDC) and Young et al. (YWKWL).

Outside a radius of about 8 arcsec, the luminosity profiles are well fitted by an $r^{1/4}$ law (Fig. 3). There are somewhat bigger deviations at larger radii in the *U* and *B* profiles which may be attributed to residuals from the sky subtraction. The effective radius R_e was derived for all colours, while the core radius R_c only for the nucleus and jet-subtracted NOT frames which have a better seeing. The results are shown in Table 2. The *R*-band core radius is smaller than that derived from the *V* and *I* bands, hence it may be influenced by the strong Hα/[N II] emission lines (Boroson & Thompson 1991). As commonly found in elliptical galaxies, NGC 4486 appears to be smaller in the red bands than in the blue ones (Kormendy & Djorgovski 1989).

Fig. 4 displays the results obtained from the ellipse fitting. The parameters ellipticity ε, position angle of the major axis PA, and the Fourier coefficients a_4 and b_4 are plotted as a function of the radius. Different symbols refer to measurements in different colours. There is very good agreement between the different colour bands. The ellipticity changes quite rapidly from almost round isophotes in the central regions to a value of $\varepsilon \approx 0.20$ at a distance of about 80 arcsec from the centre. There is no significant isophote twisting apart from the central region. In addition, the Fourier coefficients a_4 and b_4 reveal no significant deviations from pure ellipses. There is marginal evidence for a dependence of ellipticity on colour at large radii. The isophotes appear to be progressively more flattened in the *UBV* data.

3.2 The jet and counterjet

The well-known jet of NGC 4486 has been the target of many investigations, covering a wide wavelength range, in

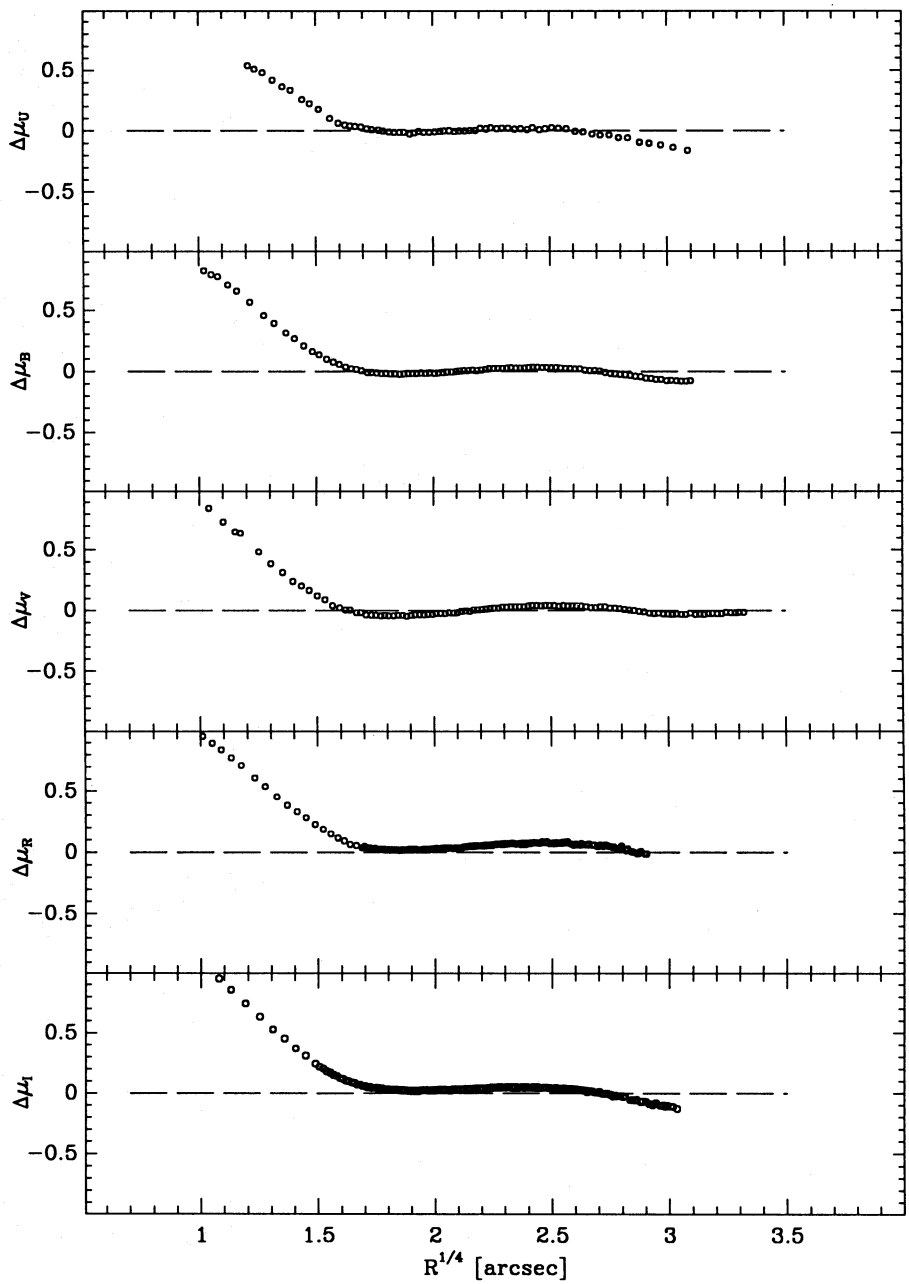

Figure 3. Residuals from the fit to the $r^{1/4}$ law for the *UBVRI* colour bands. The data are plotted as a function of distance from the galaxy centre rebinned to the $r^{1/4}$ scale.

Table 2. Core and effective radii of NGC 4486.

filter	R_c		R_e	
	[″]	[pc]	[″]	[kpc]
U	-	-	111	8.6
B	-	-	99	7.7
V	7.3	566	98	7.6
R	6.7	520	92	7.1
I	7.2	559	81	6.3

Assumed distance for NGC 4486 = 16 Mpc.

order to understand the structure and physical properties of this type of nuclear activity (see Biretta, Stern & Harris 1991 for a review of this topic). Using the results from the surface photometry, a smooth model of the galaxy was derived which was subtracted from the original images. A flux-conserving deconvolution procedure (Lucy & Baade 1989) was then applied to the subtracted images in order to improve the angular resolution. Further details and results were given by Stiavelli, Møller & Zeilinger (1991).

We have carried out the photometry at various knot complexes by determining the total flux within an aperture of 2.8-arcsec diameter. The aperture was centred on the nucleus (N) and on the knots D, E, F, A, B, C, G in each waveband. The results are shown in Table 3. Additional

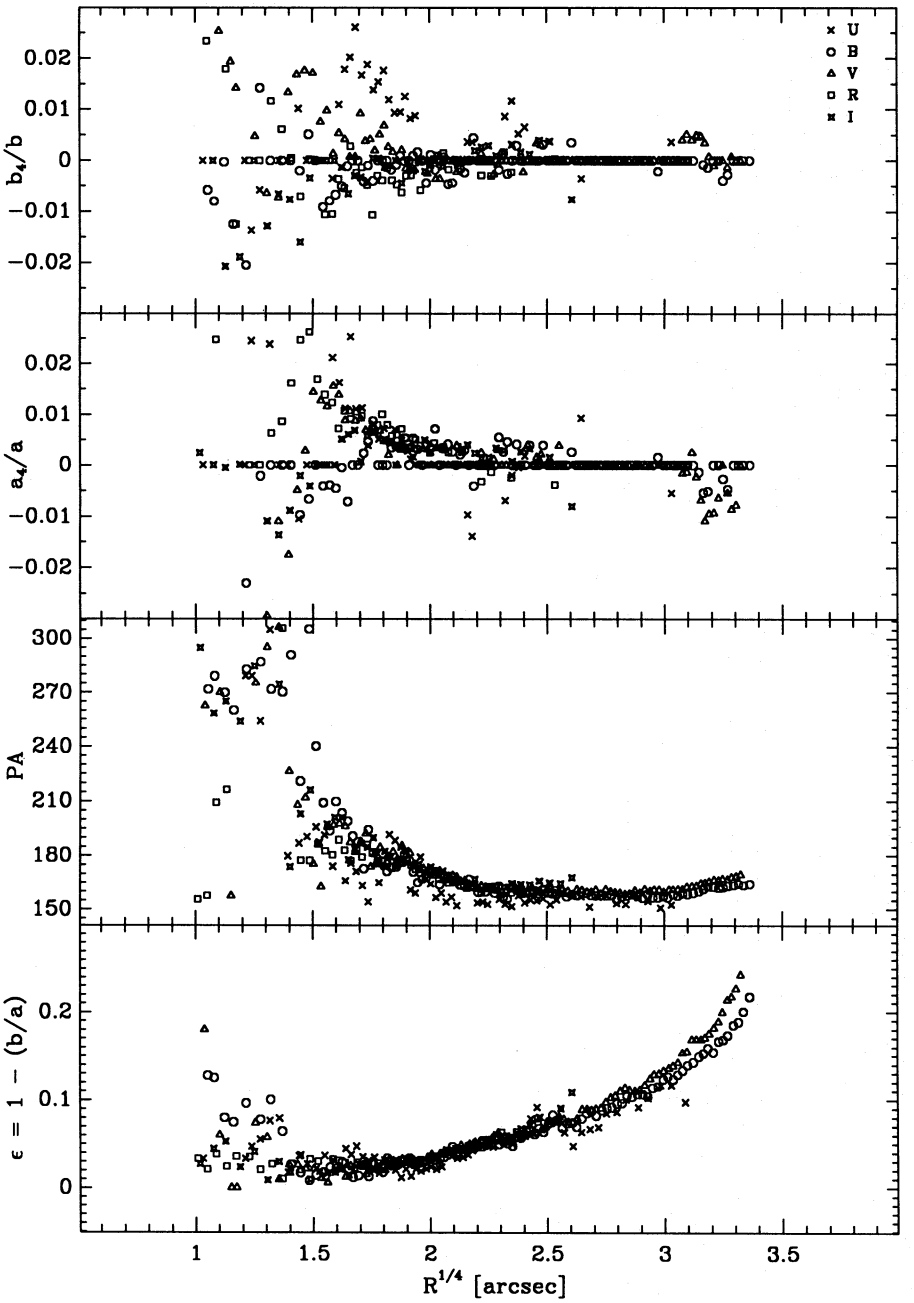

Figure 4. Ellipse fitting parameters ellipticity ϵ, position angle of the major axis PA, and the Fourier coefficients a_4 and b_4 plotted as a function of distance from the galaxy centre rebinned to the $r^{1/4}$ scale.

Table 3. Fluxes and power-law slope of the jet of NGC 4486.

knot	distance	S_ν [mJy]					slope
	["]	U (0.36μm)	B (0.44μm)	V (0.55μm)	R (0.70μm)	I (0.90μm)	
N	0.00	0.361 ± 0.016	0.435 ± 0.006	0.532 ± 0.016	0.707 ± 0.020	0.855 ± 0.022	0.96 ± 0.06
D	3.27	0.063 ± 0.010	0.054 ± 0.003	0.097 ± 0.008	0.092 ± 0.007	0.132 ± 0.008	0.85 ± 0.35
E	6.33	0.030 ± 0.010	0.040 ± 0.003	0.071 ± 0.007	0.067 ± 0.007	0.106 ± 0.007	1.27 ± 0.45
F	8.79	0.062 ± 0.010	0.076 ± 0.003	0.113 ± 0.008	0.127 ± 0.008	0.168 ± 0.009	1.05 ± 0.26
A	12.75	0.532 ± 0.020	0.653 ± 0.016	0.966 ± 0.025	1.046 ± 0.026	1.314 ± 0.032	0.94 ± 0.03
B	14.55	0.406 ± 0.017	0.538 ± 0.014	0.711 ± 0.020	0.787 ± 0.021	1.021 ± 0.026	0.92 ± 0.04
C	18.04	0.160 ± 0.010	0.222 ± 0.003	0.340 ± 0.013	0.395 ± 0.013	0.532 ± 0.016	1.24 ± 0.09
G	20.94	0.042 ± 0.010	0.066 ± 0.003	0.099 ± 0.008	0.106 ± 0.008	0.145 ± 0.008	1.22 ± 0.31

measurements using apertures with diameters of 0.6 and 1.6 arcsec were carried out in order to verify the consistency of the results. Our relatively large error estimates include various effects, such as the uncertainty in the absolute calibration and centring inaccuracy. However, an additional contribution to the uncertainty of these measurements may result from the subtraction of the galaxy itself. Despite these problems, the measurements are found to be in good agreement with previous work (Pérez-Fournon et al. 1988; Biretta et al. 1991). The spectral index $S_\nu \propto \nu^{-\alpha}$ obtained for the various positions along the jet is presented in Fig. 5. Although the power-law fit to the spectrum of the knots is not very good, the data points are compatible with a power-law fit to within 2σ. In order to detect significant variations of the spectral index along the jet, we have conducted simulations showing that variations of the spectral index are not affected by calibration errors. This allows us to use smaller errors, not including the absolute calibration uncertainty, when trying to determine a change in the spectral shape along the jet. Using this method, a constant spectral index is excluded at the 3σ level. A steepening of the spectrum is noted in particular from knot A onward, which coincides with the region where the morphology of the jet also changes. The outer jet appears broader and less focused compared to the inner region. This was noted also by Biretta et al. (1991).

The detection of the optical counterpart of a hotspot in the east radio lobe has been reported in a previous paper (Stiavelli et al. 1992). It was suggested on the basis of the derived radio-to-optical spectral index of 0.88 ± 0.01, and the evident morphological similarity, that the emission in the optical is due to synchrotron radiation. A similar conclusion was reached by Sparks et al. (1992) using optical polarization measurements. There is evidence that the spectral index increases in the immediate surroundings of the hotspot. This result was reported at the 2σ level by Stiavelli et al. (1992) who compared the NOT *I*-band image with 2-cm VLA radio data. The analysis of the combined EFOSC2 Gunn *i*- and NOT *I*-band images confirms this at the 3σ level. In the picture which explains the hotspot as being due to the presence of an unseen counterjet which continuously feeds the hotspot region, the observed increase of the spectral index may be explained in terms of the shorter synchrotron-loss lifetime for the higher energy relativistic electrons supplied by the counterjet at the hotspot location.

3.3 The core region

The core region of NGC 4486 has been the subject of several detailed studies, since it was known to contain a central cusp in luminosity which was originally interpreted in terms of a massive black hole (Young et al. 1978). This idea was further supported by Sargent et al. (1978) who detected an unusual rise of the stellar velocity dispersion in the core region. More recent velocity-dispersion measurements (Dressler & Richstone 1990; Jarvis & Peletier 1991; Jarvis & Melnick 1991; Carter & Jenkins 1992), however, yield discrepant results. The progress of the photometric analysis of the core region was hampered for a long time by the lack of high-resolution data. Lauer et al. (1992) studied the core region with a resolution of ≈ 0.04 arcsec using *V* and *I* images obtained with the *HST* Planetary Camera. The luminosity cusp remains still unresolved with a core radius of $R_c < 1$ pc. This seems to confirm the black hole model by Young et al. (1978), and to rule out the alternative interpretation of a dense stellar cluster proposed by Jarvis & Melnick (1991).

Sparks, Laing & Jenkins (1988) reported that in the region $3 < r < 8$ arcsec the apparent major axis of isophotes is perpendicular to the jet. There is also some evidence for the major axis being perpendicular to the jet axis in the position-angle profile of our data (Fig. 4). However, as there appear to be differences in the various colour bands, these results may be influenced by the presence of dust. Indeed, when a smooth model of the galaxy is subtracted from the galaxy images, some of the well-known Hα filaments show up as negative-level stripes, indicating that the Hα filaments contain dust which absorbs the galaxy light. We used the NOT *I* band for a more detailed isophote analysis of the core regions in order to minimize the effect of these disturbances. The images were analysed by two different approaches, which gave consistent results. First, the unresolved nuclear component was subtracted from the co-added *I*-band image as described previously. Secondly, the *I*-band frame with the best seeing (0.52 arcsec FWHM) was cleaned by means of an adaptive filter which is dependent on the intensity gradients in user-selected image areas. The fitting of the isophotes on the two final images was performed with various algorithms (Stiavelli et al. 1991) in order to ensure the reliability of the results.

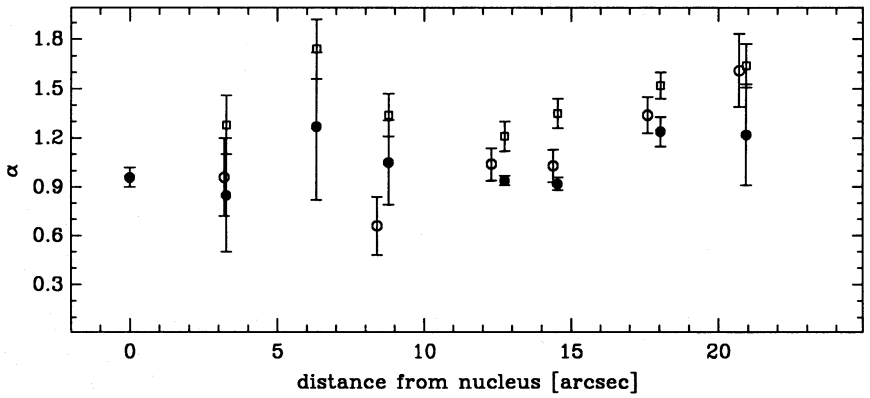

Figure 5. The average spectral index as a function of position along the jet (filled circles). As reference the respective data of Biretta et al. (open squares) and Pérez-Fournon et al. (open circles) are plotted.

Due to the evident roundness of the isophotes, the position angle of the major axis is very sensitive to deformations of the galaxy isophotes introduced by artefacts. Nevertheless, a good agreement between the different sets of measurements was found. In Fig. 6 the ellipticity and position-angle profiles of the central 15-arcsec region are presented. These results were obtained with the fitting algorithm described by Bender & Möllenhoff (1987) incorporated in the ESO MIDAS package. In the core region ($r < 3.5$ arcsec) a rapid change in the position-angle profile is noted. Inside this region the isophotes tend to align with the jet (PA$\approx 290°$), while outside this radius ($3.5 < r < 20$ arcsec) the position angle changes to $\approx 180°$. The fact that this sharp discontinuity is verified independently by various algorithms on two different images suggests that this is intrinsic to the galaxy and not an artefact introduced by the data-analysis procedure. Since the ellipticity remains constant in the inner region, one may also conclude that there are no significant residuals from the core subtraction.

The colours of the nucleus are $(B-V)=0.39\pm0.2$, $(V-R)=0.56\pm0.1$ and $(V-I)=1.0\pm0.1$. When compared to the colours immediately outside the nuclear region, we observe an excess in $(B-V)$ and $(V-I)$. The subtraction of the nucleus in the U and B bands is less reliable, since these images were taken in conditions of worse seeing. Taken at face value, the $(U-B)$ nuclear colour is about -0.7. The nuclear spectral shape is rather well fitted by a power law, but, if we attempt to model the observed B, V, R and I nuclear fluxes as a simple superposition of stellar light plus a non-thermal power-law contribution, no solution can be found for a stellar light dominated spectrum; this means that either the emission is simply a featureless power-law continuum or that dust and/or a contribution from line emission must be important.

We have constructed two simple models, based on the Jeans equations (Binney & Tremaine 1987), to verify qualitatively that the luminosity profile derived by us is in agreement with the velocity-dispersion profile of Jarvis & Peletier (1991) which shows a decrease in velocity dispersion in the inner 2 arcsec. The results are shown in Fig. 7. The first model assumes a constant mass-to-light ratio and a velocity dispersion which is isotropic in the centre and anisotropic at larger radii. This model is not substantially different from the one proposed by Binney & Mamon (1982). Note that the dip in velocity dispersion is produced even in isotropic models. Radial anisotropy is involved only in producing a decreasing velocity-dispersion profile outside 2 arcsec. The second model assumes that a black hole is present ($M_{BH} = 5.7\times10^9$ $M_\odot$) and is responsible for the observed decrease in velocity dispersion outside 2 arcsec. Here tangential orbits are needed close to the black hole to produce the observed dip, and the system is characterized by purely tangential orbits up to about 2 arcsec in radius. A very steep rise in velocity dispersion is expected at very small radii, but such a rise would probably be washed out by seeing effects, since it is confined to radii smaller than 0.4 arcsec and involves only 5 per cent of the stellar mass inside 2 arcsec.

4 CONCLUSIONS

We have performed high-resolution *UBVRI* surface photometry on NGC 4486 and derived the geometric isophote

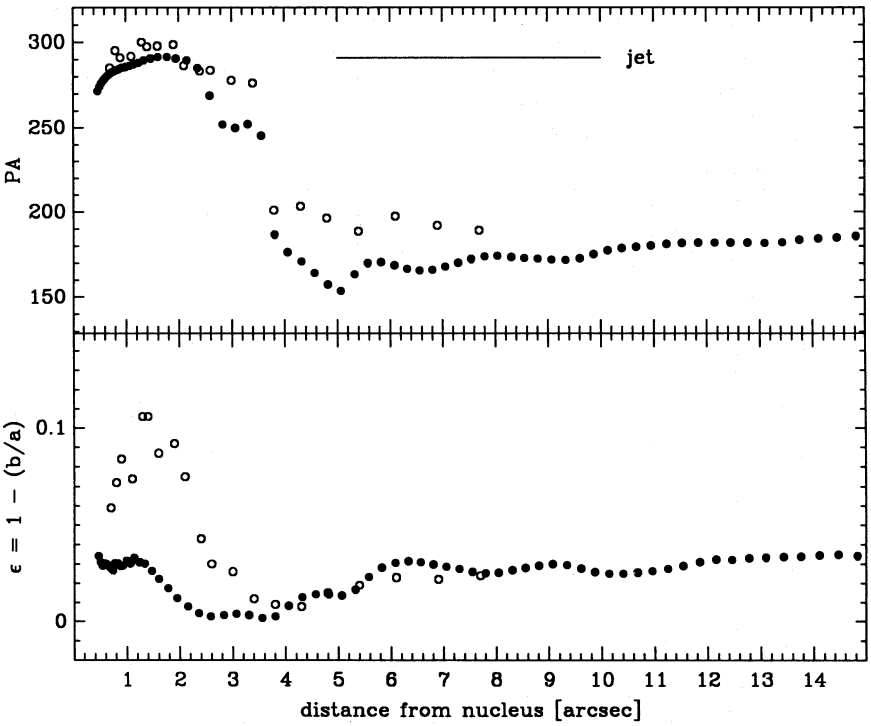

Figure 6. Ellipse fitting parameters ε and PA as a function of radius for the core region of NGC 4486 obtained from the *I*-band image. The measurements of Sparks et al. are indicated by open circles. The bar labelled 'jet' indicates the position angle of the jet axis.

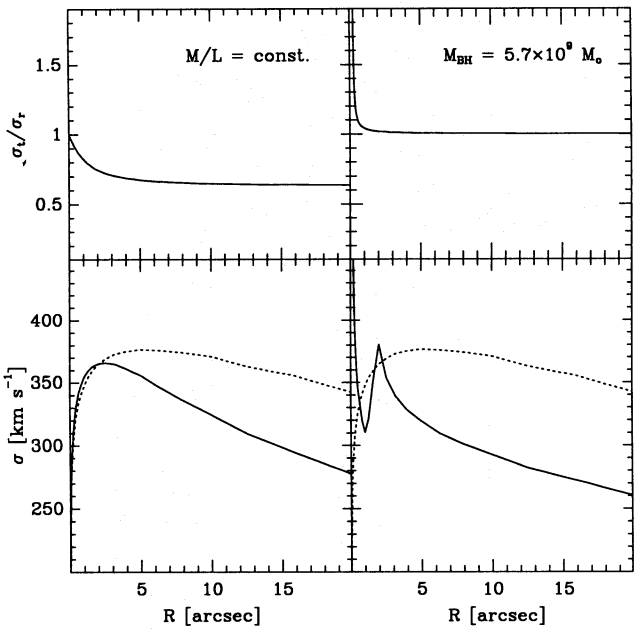

Figure 7. The upper panels show the velocity anisotropy σ_t/σ_r and the lower panels the predicted velocity-dispersion profile for two models constructed from the observed *I*-band luminosity profile. The model shown in the left-hand panel was created with a constant M/L ratio and a radially biased velocity dispersion. The model shown in the right-hand panel has a massive black hole and tangentially biased orbits close to the centre. Both models present a central dip in velociy dispersion. The dotted line represents the velocity dispersion profile of an isotropic model (without black hole component).

parameters and colour gradients. Subtracting the contribution of the unresolved nuclear component and the prominent jet, we could study at high resolution the very central parts of the galaxy. The surface photometry reveals a 'normal' elliptical galaxy. The comparison with data available in the literature shows clearly the limits of accuracy one may achieve.

Because of its proximity, NGC 4486 has been one of the key objects for studying non-thermal activity. By subtracting a smooth galaxy model and applying a flux-conserving deconvolution procedure, we have been able to isolate the jet structure, making evident the similarity of optical and radio jets down to small-scale structures (Stiavelli et al. 1991). The jet may be explained as a hollow, cone-like structure with emission filaments wound around which give rise to the limb-brightening. In the inner region the energy seems to propagate essentially loss-free until it encounters external material at knot A. From knot A onward the morphology of the jet changes drastically, appearing more diffuse with the knots being arranged in a wavy pattern. This coincides with a change in the spectral index at knot A indicating a change in the emission mechanism.

The discovery of the optical counterpart of the east radio lobe hotspot (Stiavelli et al. 1992; Sparks et al. 1992), which is found to be merely an extension of the radio synchrotron spectrum, together with the short lifetime of the optically emitting synchrotron electron, implied the presence of an unseen counterjet. Since NGC 4486 was considered until now to be one of the prototype one-sided jet radio galaxies, this raises the obvious question whether perhaps all of these objects possess symmetric jet structure. The detected variations of the spectral index in the immediate neighbourhood of the hotspot strengthen the counterjet hypothesis.

The isophotes of the stellar component show a significant amount of twisting at about 3 arcsec from the centre. In the centre the isophotes appear to be aligned with the jet axis and are then found to change rapidly until the major axis of the isophotes is almost perpendicular to it. This seems to indicate that there is a connection between the process responsible for the jet structure and the geometry of the galaxy potential. Using geometric considerations, Sparks et al. (1988) explained the shape of the core as an oblate spheroid whose plane is perpendicular to the jet.

We have also discussed the properties of the non-thermal nucleus on the basis of available data. The question of its nature remains still open. The observed central dip in the inner 2-arcsec region, where the stellar velocity dispersion is about 50 km s^{-1} lower than in the rest of the galaxy (Jarvis & Peletier 1991; Carter & Jenkins 1992), may be reproduced both by models with constant M/L and by the presence of a black hole ($M_{BH} = 5.7 \times 10^9$ $M_\odot$) using as a basis the derived *I*-band luminosity profile. However, our black hole model predicts a very steep rise of the velocity dispersion in the inner 0.4-arcsec region. Our conclusion is that the present kinematic data cannot confirm nor exclude the presence of a supermassive black hole in the core of M87, although the central dip in velocity dispersion renders models with such a supermassive black hole somewhat less attractive.

ACKNOWLEDGMENTS

The authors thank R. F. Peletier and the anonymous referee for useful comments which helped to improve this paper.

REFERENCES

Bender R., Möllenhoff C., 1987, A&A, 177, 71
Binney J., Mamon G., 1982, MNRAS, 200, 361
Binney J., Tremaine S., 1987, in Ostriker J. P., ed., Galactic Dynamics. Princeton Univ. Press, Princeton, p. 195
Biretta J. A., Stern C. P., Harris D. E., 1991, AJ, 101, 1632
Boroson T. A., Thompson I. B., 1991, AJ, 101, 111
Boroson T. A., Thompson I. B., Shectman S. A., 1983, AJ, 88, 1707
Carter D., Dixon K. L., 1978, AJ, 83, 574
Carter D., Jenkins C. R., 1992, preprint
Davis L. E., Cawson M., Davies R. L., Illingworth G. D., 1985, AJ, 90, 169
de Vaucouleurs G., Nieto J.-L., 1978, ApJ, 220, 449
de Vaucouleurs G., Nieto J.-L., 1979, ApJ, 230, 697
Dressler A., Richstone D. O., 1990, ApJ, 348, 120
Jarvis B. J., Melnick J., 1991, A&A, 244, L1
Jarvis B. J., Peletier R. F., 1991, A&A, 247, 315
Jedrzejewski R. I., 1987, MNRAS, 226, 747
Kjeldsen H., 1990, Test of the Stockholm CCD camera on the NOT adaptor, internal report (Stockholm Observatory)
Kormendy J., Djorgovski S., 1989, ARA&A, 27, 235
Landolt A. U., 1985, AJ, 88, 439
Lauer T. D. et al., 1992, AJ, 103, 703
Longo G., de Vaucouleurs A., 1983, A general catalogue of photoelectric magnitudes and colors in the U, B, V system. Monographs in Astronomy No. 3, Univ. Texas, Austin

Longo G., de Vaucouleurs A., 1985, Supplement to the general catalogue of photoelectric magnitudes and colors in the U, B, V system. Monographs in Astronomy No. 3A, Univ. Texas, Austin

Lucy L. B., Baade D., 1989, in Grosbøl P. J. et al., eds, 1st ESO/ST-ECF Data Analysis Workshop. ESO, Garching, p. 219

Peletier R. F., Davies R. L., Illingworth G. D., Davis L. E., Cawson M., 1990, AJ, 100, 1091

Pérez-Fournon I., Colina L., González-Serrano J. I., Biermann P. L., 1988, ApJ, 329, L81

Prugniel P., 1989, in Grosbøl P. J. et al., eds, 1st ESO/ST-ECF Data Analysis Workshop. ESO, Garching, p. 161

Sargent W. L. W., Young P. J., Boksenberg A., Shortridge K., Lynds C. R., Hartwick D. A., 1978, ApJ, 221, 731

Sparks W. B., Laing R. A., Jenkins C. R., 1988, AJ, 95, 1684

Sparks W. B., Fraix-Burnet D., Macchetto F., Owen F. N., 1992, Nat, 355, 804

Stiavelli M., Møller P., Zeilinger W. W., 1991, Nat, 354, 132

Stiavelli M., Biretta J. A., Møller P., Zeilinger W. W., 1992, Nat, 355, 802

Stiavelli M., Prugniel P., Zeilinger W. W., 1991, in Grosbøl P. J., Warmels R. H., eds, 2nd ESO/ST-ECF Data Analysis Workshop. ESO, Garching, p. 231

Young P. J., Westphal J. A., Kristian J., Wilson C. P., Landauer F. P., 1978, ApJ, 221, 721